Global analysis of adenylate-forming enzymes reveals β-lactone biosynthesis pathway in pathogenic *Nocardia*

Serina L. Robinson,[1,2,3] Barbara R. Terlouw,[4] Megan D. Smith,[2,3] Sacha J. Pidot,[5] Tim Stinear,[5] Marnix H. Medema,[4] and Lawrence P. Wackett[1,2,3]

[1]Graduate Program in Bioinformatics and Computational Biology, University of Minnesota 111 S. Broadway, Suite 300, Rochester, MN, 55904, USA; [2]Graduate Program in Microbiology, Immunology, and Cancer Biology, University of Minnesota, 689 23rd Ave SE, Minneapolis, MN, 55455, USA; [3]BioTechnology Institute, University of Minnesota, 1479 Gortner Avenue, Saint Paul, MN, 55108, USA; [4]Bioinformatics Group, Wageningen University & Research, Droevendaalsesteeg 1, 6708 PB, Wageningen, the Netherlands; [5]Department of Microbiology and Immunology at the Doherty Institute, University of Melbourne, 792 Elizabeth St, Melbourne, VIC, 3000 Australia

Running title: Global analysis of adenylate-forming enzymes

Keywords: natural product biosynthesis, acetyl-CoA synthetase, enzyme catalysis, bioinformatics, machine learning, coenzyme A, adenylation enzymes, *Nocardia,* substrate specificity, β-lactone synthetases

ABSTRACT

Enzymes that cleave ATP to activate carboxylic acids play essential roles in primary and secondary metabolism in all domains of life. Class I adenylate-forming enzymes share a conserved structural fold but act on a wide range of substrates to catalyze reactions involved in bioluminescence, nonribosomal peptide biosynthesis, fatty acid activation, and β-lactone formation. Despite their metabolic importance, the substrates and catalytic functions of the vast majority of adenylate-forming enzymes are unknown without tools available to accurately predict them. Given the crucial roles of adenylate-forming enzymes in biosynthesis, this also severely limits our ability to predict natural product structures from biosynthetic gene clusters. Here we used machine learning to predict adenylate-forming enzyme function and substrate specificity from protein sequence. We built a web-based predictive tool and used it to comprehensively map the biochemical diversity of adenylate-forming enzymes across >50,000 candidate biosynthetic gene clusters in bacterial, fungal, and plant genomes. Ancestral enzyme reconstruction and sequence similarity networking revealed a 'hub' topology suggesting radial divergence of the adenylate-forming superfamily from a core enzyme scaffold similar to contemporary aryl-CoA ligases. Our classifier also predicted β-lactone synthetases in novel biosynthetic gene clusters conserved across >90 different strains of *Nocardia*. To test our computational predictions, we purified a candidate β-lactone synthetase from *Nocardia brasiliensis* and reconstituted the complete biosynthetic pathway in vitro to link the gene cluster to the β-lactone natural product, nocardiolactone. We anticipate our machine learning approach will aid in functional classification of enzymes and advance natural product discovery.

Introduction

Adenylation is a widespread and essential reaction in nature to transform inert carboxylic acid groups into high energy acyl-AMP intermediates. Class I adenylate-forming enzymes are involved in natural product biosynthesis, firefly bioluminescence, and the activation of fatty acids with coenzyme A. The conversion of acetate to acetyl-CoA by a partially purified acetyl-CoA ligase was first described by Lipmann in 1944 (*1*). Since then, enzymes with this conserved structural fold have been found to activate over 200 different substrates including aromatic, aliphatic, and amino acids. To encompass the major functional enzyme classes, the 'ANL' superfamily was proposed based on the Acyl-CoA ligases, Nonribosomal peptide synthetases (NRPS), and Luciferases (*2*).

Most ANL superfamily enzymes catalyze two-step reactions: adenylation followed by thioesterification. During the thioesterification step, ANL enzymes undergo a dramatic conformational change involving a 140° domain rotation of the C-terminal domain (*2*). Thioester bond formation results from nucleophilic attack, typically by a phosphopantetheine thiol group. A notable exception to phosphopantetheine is the use of molecular oxygen by firefly luciferase to convert D-luciferin to a light-emitting oxidized intermediate. Other interesting exceptions include functionally-divergent ANL enzymes within the same pathway that catalyze the adenylation and thioesterification partial reactions separately (*3, 4*). The ANL superfamily has recently expanded to include several new classes of enzymes including the fatty-acyl AMP ligases (*5*), aryl polyene adenylation enzymes (*6, 7*), and β-lactone synthetases (*8*). Strikingly, an ANL enzyme in cremeomycin biosynthesis was shown to use nitrite to catalyze late stage N-N bond formation in diazo-containing natural products (*9*). The discovery of such novel enzymatic reactions nearly 75 years after the Lipmann's initial report suggests the ANL superfamily still has unexplored catalytic potential, particularly in specialized metabolism.

No computational tools currently exist for prediction and functional classification of ANL enzymes at the superfamily level. Still, the development of one previous platform, which is no longer supported or available, showed that this class of enzymes is amenable to computational predictions of substrate and function (*10*). Previously, bioinformatics tools were also developed to predict substrates for NRPS adenylation (A) domains (*11, 12*). Genome mining approaches using NRPS A domain prediction tools have proved useful to access the biosynthetic potential of unculturable organisms and link 'orphan' natural products with their biosynthetic gene clusters. For example, NRPS A domain predictions guided the discovery of the biosynthetic machinery for the leinamycin family of natural products (*13*) and enabled sequence-based structure prediction of several novel lipopeptides by Zhao et al. (*14*). However, Zhao et al. reported limitations in existing tools in that they could not predict the chain length of lipid tails incorporated into lipopeptides. Lipid tails are prevalent in natural products and are incorporated by fatty acyl-AMP-or CoA-ligase enzymes, both in the ANL superfamily. These enzymes are among the most well-studied subclasses of ANL enzymes. For less-studied subclasses, enzyme functions and substrates are even more challenging to predict. Hence, a computational tool encompassing all classes of ANL enzymes would constitute a major step towards more accurate structural prediction of natural product scaffolds.

Here, we used machine learning to develop a predictive platform for ANL superfamily enzymes and map their substrate-and-function landscape across 50,064 candidate biosynthetic gene clusters in bacterial, fungal, and plant genomes. We detected candidate β-lactone synthetases in uncharacterized biosynthetic gene clusters from pathogenic *Nocardia* spp. and experimentally validated the gene cluster in vitro to link it to the orphan β-lactone compound, nocardiolactone. Overall, this research provides a proof-of-principle towards the use of machine learning for classification of enzyme substrates to guide natural product discovery.

Results

Machine learning can accurately predict ANL enzyme function and substrate specificity

A global analysis of protein family domains revealed that ANL superfamily enzymes (PF00501; AMP-binding domains) are the third most abundant domain in known natural product biosynthetic pathways (Table S1). Despite the essential and varied roles of ANL enzymes, there is no database that catalogs their biosynthetic diversity. Therefore, we mined the literature, MIBiG (*15*), and UniProtKB (*16*) for ANL enzymes with known substrate specificities. We then constructed a training set of >1,700 ANL protein sequences paired with their functional class, substrate(s), kinetic data, and crystal structures if solved. As reported previously by Gulick and others, ANL superfamily enzymes in our training set were divergent at the sequence level but shared a common structural fold and core motifs including (Y/F)(G/W)X(A/T)E and (S/T)GD critical for ATP-binding and catalysis (*2*).

We defined nine major functional enzyme classes on the basis of having multiple experimentally-characterized enzymes per class: short chain acyl CoA synthetases (C_2 – C_5, SACS), medium chain acyl-CoA synthetases (C_6 – C_{12}, MACS), long chain acyl-CoA synthetases (C_{13} – C_{17}, LACS), very-long chain and bile acyl-CoA synthetases (C_{18+}, VLACS), fatty acyl-AMP ligases (FAAL), luciferases (LUC), β-lactone synthetases (BLS), aryl-CoA ligases (ARYL), and NRPS A domains (NRPS). In addition, we trained a separate model to predict enzyme substrate specificity. While prediction at the level of an individual substrate is desirable, the broad specificity of some classes of ANL enzymes required the formation of substrate groups. For example, one class of LACS demonstrated activity with fatty acids with chain lengths ranging from C_8 – C_{20} (17). Furthermore, there were over 200 distinct substrates in our training set, many with just one experimental example. Therefore, we clustered substrates based on chemical similarity (Tanimoto coefficient) to identify 15 groups for broad level substrate classification (Table S2).

Previously, 34 amino acids within 8 Å of the gramicidin synthetase active site were shown to be critical for accurate prediction of NRPS A domain substrate specificity (*11*). Due to the high level of structural conservation between NRPS A domains and other proteins in the superfamily, we hypothesized these 34 active site residues would also be important features for ANL substrate prediction. Using an AMP-binding profile Hidden Markov Model (pHMM), we extracted 34 active site residues from our >1,700 training set sequences. Further inspection of the superfamily-wide pHMM alignment revealed the presence of a fatty acyl-AMP ligase-specific insertion (FSI) of 20 amino acids not present in other superfamily members (Fig. S1). The FSI has been suggested to inhibit the 140° domain rotation of the C-domain and is critical for the rejection of CoA-SH as an acceptor molecule (*5*). Since the FSI is known to be an important feature to distinguish FAAL from LACS enzymes, we extracted 20 FSI residues from each sequence and appended them to our feature vector for a total of 54 residues. Each amino acid was further encoded as 15 normalized real numbers corresponding to different physicochemical properties including hydrophobicity, volume, secondary structure, and electronic properties (*11*). The physicochemical properties were then used to train machine learning models to predict enzyme function and substrate (Fig. 1A).

Three different machine learning algorithms were evaluated for our classification problem: feed-forward neural networks, naïve Bayes, and random forest. Random forest performed slightly better than its counterparts for both function and substrate classification problems (Figure 1B). Naïve Bayes also performed well, but was significantly slower than random forest in run-time. The feed forward neural network performed the worst, likely due to a relatively small number of training samples, and was also the slowest model to train. On the basis of speed and accuracy we chose to proceed with the random forest algorithm. Our best performing model achieved 82.5 ± 2.3% test set classification accuracy for substrate specificity and 83.1 ± 2.2% for functional class prediction (Fig. 1B; Fig. S2). The average area under the curve (micro-average AUC) was 0.981 for substrate group prediction and 0.973 for functional class (Fig. 1C; Fig. S2). Within-class accuracy was highest for the NRPS A domains, most likely due to a large amount of experimental data for this protein family (Fig. S2). Both of our classifiers also performed well with highly-specialized enzymes that accept

single substrates such as the BLS and LUC classes (Fig. S2). We speculate that enzymes with more specialized functions might have a distinct 'active site pattern' that could be learned by our classifier due to the evolutionary selection and preference of these enzymes for single unique substrates (e.g. D-luciferin). Our classifier consistently performed the worst on substrate classification for enzymes with broad substrate specificity such as the aryl/biaryl acids and $C_6 - C_{11}$ chain length fatty acids and aryl acids (Fig. 1D).

We developed a web application, AdenylPred (z.umn.edu/AdenylPred), for **Adenyl**ation **Pred**iction to make our machine learning models publicly available. Users can upload their sequences of adenylate-forming enzymes in multi-FASTA or GenBank format either as nucleotide or protein sequences. Predictions and probability scores are reported for both functional classification and substrate specificity. The entire ANL enzyme training set is also available in a searchable database format. Overall, the web app is an accessible front end for users with little computational experience. A command-line version of the tool (https://github.com/serina-robinson/adenylpred) is recommended for the analysis of large datasets and advanced users.

Specialized ANL enzymes may have evolved from an ancestral scaffold utilizing CoA-SH

We next used a phylogenetic approach to investigate the functional divergence of ANL superfamily enzymes (Fig. 2). Maximum-likelihood phylogenetic analysis revealed that some functional classes, including the BLS, LUC, and NRPS enzymes, formed tight monophyletic clades whereas others, mainly enzymes in the ARYL class, were dispersed throughout the tree. The wide phylogenetic distribution of the ARYL sequences indicated many ARYL enzymes were more closely related to different protein subfamilies than to each other. This observation could be explained by two evolutionary scenarios: 1) aryl-CoA ligase activity arose independently several times throughout ANL superfamily evolution or 2) radial divergence of the superfamily occurred from an ancestral scaffold similar to contemporary ARYL enzymes (*18*). To investigate these scenarios further, we used a maximum-likelihood ancestral reconstruction approach to estimate the 10 most likely sequences for the predicted ancestral protein at the root of the ANL phylogeny (*19*). We then used AdenylPred to extract sequence features and predict function and substrate for our reconstructed ancestral proteins. AdenylPred classified 10/10 of the most likely ancestral reconstructions of the root node as aryl-CoA ligases most likely to activate aryl and biaryl derivatives as substrates (probability = 0.6). We also tested a maximum-likelihood ancestral reconstruction using only 34 active site residues as the seed sequences rather than full sequences and obtained similar ARYL predictions (probability = 0.7). These findings suggest that the active sites of our reconstructed ancestral ANL proteins were most similar to contemporary ARYL enzymes.

Sequence similarity networking reveals a 'hub' network topology

To build a global picture of the distribution of adenylate-forming enzymes in biosynthetic gene clusters, we applied AdenylPred to a taxonomically diverse and comprehensive collection of bacterial, fungal, and plant genomes. We extracted 50,064 standalone adenylate-forming enzyme sequences from candidate biosynthetic gene clusters detected using antiSMASH (*20*), fungiSMASH (*21*), and plantiSMASH (*22*). To visualize results, we constructed a sequence similarity network with sequences colored by their functional classification using AdenylPred (Fig. 3A). The sequence similarity network displayed a 'hub-and-spoke' topology in which most functional protein subfamilies showed higher sequence similarity with 'hub' sequences than with any other subfamily (Fig. 3A). The hub nodes were mainly comprised of aryl-CoA ligases. To test the robustness of this topology with a different sequence set, we constructed a sequence similarity network from a smaller set of all AMP-binding domains from the curated MIBiG database (Fig. S3). Again, we recovered the same topology with the aryl-CoA ligases at the center. Of the 48,250 full length AMP-binding hits that we analyzed with AdenylPred, the majority were predicted to be in the ARYL and NRPS classes (Fig. 3B). There were no predicted luciferases in

the AMP-binding hits which was expected since firefly genomes were not included in the dataset. Interestingly, the predicted FAALs outnumbered LACS more than tenfold (3,673 to 322). Since both FAALs and LACSs both accept long-chain fatty acids as substrates, these findings support previous findings that the majority of lipid tails in lipopeptides and other natural products may be incorporated through FAAL-mediated activity rather than CoA-activation (*23*). CoA-activation of long and very long chain fatty acids and β-lactone formation were the least common functions predicted to occur among ANL enzymes in biosynthetic gene clusters (Fig. 3B).

AdenylPred-guided discovery of β-lactone synthetases in biosynthetic gene clusters

β-Lactone synthetases were the most recently discovered members of the ANL superfamily and their prevalence in natural product biosynthetic gene clusters has never been characterized. To probe their distribution, we examined AdenylPred hits for β-lactone synthetases from our collection of 50,064 candidate biosynthetic gene clusters. As expected, we detected β-lactone synthetase hits in gene clusters corresponding to known β-lactone products ebelactone and lipstatin (*24, 25*). We also predicted multiple uncharacterized β-lactone synthetases in *Nocardia* genomes. Only one β-lactone natural product from *Nocardia* spp., nocardiolactone, has been isolated to date (*26*). No follow-up studies on nocardiolactone were published and the biosynthetic gene cluster was never reported.

We identified three flanking genes around the predicted β-lactone synthetase genes in *Nocardia spp.* that shared synteny with biosynthetic genes for the β-lactone natural product, lipstatin (Fig. 4A). The lipstatin cluster encodes NRPS and formyltransferase enzymes that attach an *N*-formyl leucine to the di-alkyl backbone *(23)*. Notably, NRPS and formyltransferase genes were absent from all candidate clusters in *Nocardia* (Fig. 4B). We hypothesized that this minimal set of biosynthetic genes, termed *nltABCD*, encode the necessary enzymes for *Nocardia* spp. to produce a di-alkyl β-lactone product similar to lipstatin but lacking an amino acid side chain. Predicted functions of genes in the *nltABCD* operon matched the orphan structure of the β-lactone product, nocardiolactone (Fig. 4A), leading us to test our hypothesis experimentally.

In vitro reconstitution of the nocardiolactone pathway links biosynthetic gene cluster to its orphan natural product

Nocardiolactone was originally isolated in 1999 from a pathogenic strain of *Nocardia brasiliensis* and other unidentified strains of *Nocardia* spp., none of which are available in public culture collections (*26*). Genetic manipulation in *Nocardia* is challenging therefore we opted instead to reconstitute the complete biosynthetic pathway in vitro by heterologously expressing and purifying individual *nltABCD* pathway enzymes. This approach gave us full control to analyze enzyme function through direct biochemical analysis of intermediates and comparison to authentic standards.

We cloned and expressed a candidate β-lactone synthetase, termed NltC, from a publicly available *N. brasiliensis* genome. NltC purified as a 60 kilodalton (kDa) monomer. To test β-lactone synthetase activity, we incubated NltC, ATP, and $MgCl_2$ with *syn*- and *anti*-2-octyl-3-hydroxydodecanoic acid diastereomers as substrate mimics (Fig. 5A). We observed NltC-catalyzed formation of *cis*-and *trans*-β-lactones after overnight reaction compared to no enzyme controls (Fig. S4A). The coupling constants were consistent with synthetic standards for *cis*- and *trans*-β-lactones of comparable chain length. AMP release is also commonly used as a readout for ANL superfamily activity. In a time-course analysis of AMP release by NltC, we observed activity with C_{20} chain length β-hydroxy acids but no activity with C_{14} length analogs above the level of the no-substrate control (Fig. 5A). NltC also showed weak activity with 2-hexyldecanoic acid as a substrate mimic, but not with 10-nonadecanol, suggesting adenylation of the carboxylic acid occurs rather than hydroxyl group (Fig. S4B). These results are consistent with the reported adenylation activity of for the β-lactone synthetase from *Xanthomonas campestris* and with the ANL superfamily (*27*). Overall, these results confirmed our AdenylPred-guided

prediction that NltC in *N. brasiliensis* is a functional β-lactone synthetase.

To further confirm the role of NltC in nocardiolactone biosynthesis, we heterologously expressed and purified two upstream thiolase enzymes, NltA and NltB. Recently, homologous enzymes in the lipstatin biosynthetic pathway, LstA and LstB were shown to form a functional heterodimer to catalyze 'head-to-head' Claisen condensation of two acyl-CoAs (*28*). We hypothesized NltA and NltB might catalyze a similar reaction to form the nocardiolactone backbone (Fig. 5B). When heterologously expressed, NltA was mostly insoluble and formed inclusion bodies even when co-expressed with chaperones. We also attempted to purify a NltA homolog from a closely-related organism, *Nocardia yamanashiensis,* and again observed inclusion body formation. In contrast, NltB could be purified with a moderate yield (~28 mg/L of culture). Individually, NltA and NltB protein preparations did not display activity with any chain length (C_8 – C_{16}) acyl-CoA substrate tested. However, when NltA and NltB were co-expressed on a single plasmid we obtained soluble protein that actively catalyzed Claisen condensation with myristoyl-CoA as the substrate to form 2-myristoyl myristic acid (Fig. 5B). Size exclusion chromatography indicated that co-expressed NltAB eluted at approximately 72 kDa, suggesting a heterodimeric state.

From homology modeling and sequence analysis we observed that the NltB sequence was truncated and lacked a Cys-His-Asn catalytic triad similar to reports for LstB (*28*). A key glutamate residue in LstB was reported to be a critical nucleophile for LstAB catalysis, although no crystal structure is available (*28*). In the crystal structure of the physiological homodimer, OleA, from *Xanthomonas campestris*, a similarly-positioned glutamate from chain A was shown to enter the active site of chain B and abstract a proton to catalyze carbon-carbon bond formation (*29*). Based on homology modeling and structural alignments with OleA, $NltB_{E57}$ may be poised to act as a nucleophile in the NltA active site (Fig. S5A). We used site-directed mutagenesis to mutate the NltB glutamate (E57) to either alanine or glutamine. Claisen condensation activity was abolished in $NltAB_{E57A}$ and $NltAB_{E57Q}$ mutants compared to wild-type NltAB (Fig. S5B). Taken together, these results suggest NltA and NltB may form a functional heterodimer with $NltB_{E57}$ required to catalyze the Claisen condensation of two fatty acyl-CoA substrates.

The final enzyme in the nocardiolactone cluster, NltD, belongs to the short chain reductase superfamily. NltD purified as a 78 kDa fusion protein with a maltose binding protein tag. NltD has an N-terminal conserved nucleotide binding motif (Rossman fold) and a SX_nYXXXK catalytic triad characteristic of short chain reductase superfamily members. NltD shares 53% amino acid identity with the lipstatin reductase (LstD) and 36% identity with *X. campestris* OleD, a 2-alkyl-3-ketoalkanoic acid reductase involved in olefin biosynthesis (Fig. 4A). Since studies on OleD demonstrated 2-alkyl-3-ketoalkanoic acids are unstable, we monitored the reaction in reverse with 2-alkyl-3-hydroxyalkanoic acid substrates using a spectrophotometric assay for NADPH formation (*30*). Purified NltD catalyzed $NADP^+$-dependent conversion of 2-alkyl-3-hydroxyalkanoic acid to 2-alkyl-3-ketoalkanoic acid with both C_{20} and C_{14} di-alkyl β-hydroxy acid substrates at a rate similar to *X. campestris* OleD (Fig. S6). We next reconstituted the entire nocardiolactone pathway by combining purified pathway enzymes with decanoyl-CoA precursors, NADPH, ATP, and $MgCl_2$ (Fig. 5C; Fig. S7). Due to instability and loss of activity of purified NltAB over time, we improved product yield through substitution of the functionally-equivalent and stable homodimer, OleA, from *X. campestris* (*31*). After overnight incubation, we observed formation of a di-alkyl β-lactone natural product (Fig. S7). Based on in vitro evidence, we propose nocardiolactone biosynthesis is initiated via 'head-to-head' Claisen condensation of fatty acyl-CoA substrates catalyzed by a heterodimeric interaction between NltA and NltB. NltD then reduces the di-alkyl β-keto acid to a di-alkyl β-hydroxy acid in an NADPH-dependent manner. Intermolecular ring closure is catalyzed by the ATP-dependent β-lactone synthetase, NltC (Fig. 5C). Overall, these results link the *nltABCD*

biosynthetic gene cluster in *Nocardia* to the orphan natural product, nocardiolactone.

The nocardiolactone gene cluster is enriched in human pathogens

With the gene cluster established, we next probed the taxonomic distribution and abundance of the nocardiolactone pathway in *Nocardia* genomes. We used AdenylPred to identify putative β-lactone synthetases and detected *nltC* homologs with flanking *nltABD* genes in 94 out of 159 complete *Nocardia* genomes in the PATRIC database (*32*). Notably, the strict *nltABCD* cluster was not detected in any closely related genera such as *Rhodococcus, Streptomyces,* or *Mycobacterium*, suggesting nocardiolactone biosynthesis may be specific to the genus *Nocardia*. We observed the nocardiolactone gene cluster was more prevalent among strains of pathogenic clinical isolates from human patients than in strains isolated from other sources (Fig. 4). The complete *nltABCD* cluster was detected in 68% of genomes of distinct species of human pathogenic *Nocardia* relative to 27% isolated from non-human sources (p-value: 0.002, Fisher's exact test). We also queried a separate private database comprised of 169 clinical isolates of *Nocardia* from human patients (Pidot, Stinear, *in prep*) and recovered a similar proportion of complete nocardiolactone cluster hits among clinical isolates (112/169, ~66%). Although only correlative, the enrichment warrants further research and suggests a potential link between the nocardiolactone cluster and *Nocardia* pathogenicity.

Discussion

Based on our ancestral reconstruction, we propose ancient ANL enzymes had an active site most similar to contemporary enzymes that activate aryl and biaryl acids with CoA. This hypothesis is supported by the unusual 'hub' topology of the ANL network. Many other enzyme superfamilies do not have this topology and instead tend to show patterns of sequential functional divergence (*33, 34*). Babbitt and colleagues detected a similar 'hub' topology in the nitroreductase superfamily and provided multiple lines of evidence supporting that the topology indicated radial divergence of the superfamily from a minimal flavin-binding scaffold (*18*). Our results also suggest ANL sequences may have undergone radial divergence towards more specialized functions from ancestral enzymes with CoA-ligase activity.

The proposed evolutionary trajectory of the ANL superfamily is supported by experimental evidence for low-levels of CoA-ligase activity in many extant enzymes. For example, Linne et al. tested the CoA-ligase activity of five different NRPS A domains (*35*). Surprisingly, all the NRPS A domains were also able to synthesize acyl-CoAs in vitro. Enzymatic CoA-ligase activity of the NRPS A domains varied proportionally to their evolutionary similarity with a native acyl-CoA synthetase, suggesting that greater sequence divergence resulted in more specialized A domain activity and reduced bifunctionality (*35*). Firefly luciferases were also demonstrated to be bifunctional as CoA-ligases (*36*) and luciferase activity was conferred to an acyl-CoA ligase from a non-luminescent click beetle by just a single point mutation (*37*). Arora et al. showed FAAL enzymes likely lost their CoA-ligase activity due to the FSI. Indeed, deletion of the FSI conferred acyl-CoA ligase activity in FAAL28 from *Mycobacterium tuberculosis* (*5*). The fact that simple mutations can revert many enzymes back to a CoA-ligase state supports the hypothesis that the ANL superfamily arose from an ancestral enzyme using CoA-SH as an acceptor molecule. However, we cannot rule out the alternative hypothesis of CoA-ligase activity arising independently several times in the ANL superfamily. Overall, ancestral reconstruction coupled with AdenylPred analysis yielded new insights into the evolutionary structure-function relationships among adenylate-forming enzymes.

Within the ANL superfamily, the β-lactone synthetases are the newest subfamily and the extent of their role in natural product biosynthesis remains poorly understood (*8, 27*). AdenylPred detected >90 β-lactone synthetases in uncharacterized biosynthetic gene clusters which is significantly more than the eight known biosynthetic gene clusters for β-lactone natural products reported to date (*38*). The high number of predicted clusters with β-lactone synthetases relative to the few known β-lactone natural products deserves further exploration. β-Lactones

are reactive moieties that will often rapidly hydrolyze under aqueous conditions or thermally decarboxylate, thus hampering their detection (*38*). It is also plausible many biosynthetic gene clusters with β-lactone synthetases are silent. Another explanation is the potential role of β-lactones as biosynthetic intermediates to achieve other functional groups (*8*). Chemists have long referred to β-lactones as 'privileged structures' for the total synthesis of compounds with a variety of functional groups including β-lactams, gamma-lactones, and alkenes (*38, 39*). Our findings suggest microbes might also use β-lactones as intermediates since we detected a number of β-lactone synthetase hits in gene clusters known to make natural products without final β-lactone moieties such as polyunsaturated fatty acids. Indeed, β-lactone synthetases in *oleABCD* gene clusters were recently linked to production of the final alkene moiety in the biosynthesis of a C_{31} polyunsaturated hydrocarbon product (*40*). Such cases, if more widespread, may have also escaped detection because most of the predicted gene clusters with β-lactone synthetases were not detected by tools like antiSMASH *(19)* until recently, prohibiting the discovery of such biosynthetic pathways through genome mining approaches. The update of antiSMASH to detect β-lactone synthetases now enables further research into the role of β-lactones as intermediates in the biosynthesis of hydrocarbons and other secondary metabolites.

Among the predicted gene clusters with β-lactone synthetase homologs, we detected a conserved cluster in *Nocardia* which we linked to the orphan β-lactone natural product, nocardiolactone. Numerous biosynthetic gene clusters have been detected in *Nocardia* spp., and many genomes from *Nocardia* have as many type I polyketide synthases and NRPS gene clusters as *Streptomyces* genomes (*41*). Despite this, only a small number of biosynthetic gene clusters in *Nocardia* have been experimentally-verified. Recently, the biosynthetic gene cluster for the nargenicin family of macrolide antibiotics was discovered in human pathogenic strains of *Nocardia arthriditis (42)*. Khosla and colleagues also reported on a unique class of orphan polyketide synthases in the genomes of *Nocardia* isolates from human patients with nocardiosis (*43*). Based on association of this gene cluster with pathogenic clinical isolates, the authors proposed the product might play a role in infectivity in human hosts. Similarly, we found nocardiolactone clusters to be significantly more abundant in the genomes of human pathogenic strains compared to isolates from non-human sources. The enrichment supports the hypothesis that nocardiolactone and other hydrophobic natural products may play a role in virulence.

Nocardiolactone was isolated from the mycelia rather than the fermentation broth, suggesting the compound is cell-associated (*26*). The long, waxy di-alkyl tails of nocardiolactone resemble mycolic acids and would likely embed in the cell membrane. The cell wall composition varies between different species of *Nocardia* but is known to consist primarily of trehalose dimycolate and several other unidentified hydrophobic compounds (*44*). Studies on *Nocardia* virulence found that cell-surface composition was a critical determinant for attachment and penetration of host cells (*45*). Cell wall-associated lipids in *N. brasiliensis* were also shown to induce a strong inflammatory response (*44*). The role of hydrophobic natural products in *Nocardia* pathogenicity and infection remains a rich and untapped direction for future research.

In summary, we conducted the first global analysis of adenylate-forming enzymes in >50,000 candidate biosynthetic gene clusters from all domains of life. Our data-driven approach yielded evolutionary insights into superfamily divergence from a core scaffold similar to contemporary aryl-CoA ligases towards enzymes with more specialized functions such as β-lactone formation. AdenylPred analysis also detected >90 β-lactone synthetases in gene clusters in *Nocardia* spp. that were enriched in the genomes of human pathogens. Through in vitro pathway reconstitution, we were able to link this gene cluster family to the orphan natural product nocardiolactone. These findings demonstrate how machine learning methods can be used to pair gene clusters with orphan secondary metabolites and advance understanding of natural product biosynthesis.

Materials and Methods

Sequence similarity network Candidate biosynthetic gene clusters from >24,000 bacterial genomes in the antiSMASH database version 2 (*46*) were combined with precalculated plantiSMASH output (*22*) and results from fungiSMASH analysis of 1,100 fungal genomes (accession numbers available at https://github.com/serina-robinson/adenylpred_analysis/). The AMP-binding pHMM (PF00501) was used to query all genes in the dataset with default parameters, returning 213,993 significant hits. Since the distribution and identity of NRPS adenylation domains have already been analyzed in detail by Chevrette et al. (*12*), we opted to analyze only standalone AMP-binding pHMM hits. All sequences with a condensation domain (PF00668) in the same coding sequence were filtered out, leaving 71,331 'standalone' AMP-binding HMM hits. Of these, partial sequences (less than 150 amino acids in length) were removed for a total of 63,395 sequences. Due to computational limitations of visualizing large networks, the sequences were clustered using CD-HIT with a word size of 2 and 40% sequence similarity cut-off to yield 2,344 cluster representatives (*47*). Cluster representatives were combined with the AdenylPred training set sequences to observe their relation to sequences with known specificity. A sequence similarity network was created by calculating pairwise BLAST similarities between all sequences. The network was constructed and trimmed over a comprehensive range of e-value cutoffs and visualized in R using the 'igraph' package (*48*).

Training set construction The AdenylPred training set was constructed from three databases: UniProtKB, MIBiG, and the most up-to-date NRPS A domain training set from SANDPUMA (*12*). AMP-binding enzymes (PF00501) in the UniProtKB database that had experimental evidence at the protein level were extracted and linked to their substrate through literature mining and manual curation. The MIBiG database was queried with the AMP-binding HMM (PF00501). MIBiG sequences were extracted and linked to their product and substrate when reported in the literature. The SANDPUMA NRPS A domain dataset was randomly down-sampled with stratification by substrate class to balance the training set classes for substrate and enzyme function prediction. Training set sequences were grouped into 15 substrate groups and 9 enzyme functional classes. The complete training set is available through the web-application (z.umn.edu/adenylpred).

Machine learning methods Protein sequences in the training set were aligned with the AMP-binding HMM using HMMAlign (*49*). 34 substrate residues within 8 Å of the active site and the FSI were extracted and encoded as tuples of physicochemical properties as described by Roettig et al. (*11*). Three different machine learning algorithms were trained for multiclass classification: random forest, naïve Bayes, and feed forward neural networks. The data were split with stratified sampling into 75% training and 25% test sets. Tuning parameters for all models were adjusted by grid search using 10-fold cross validation repeated with 5 iterations. The confidence of random forest predictions can be assessed using a nonparametric probability estimation for class membership calculated as a value between 0 and 1 (*50*). Based on the distribution of prediction probabilities, we set an empirical threshold for prediction confidence of 0.6 (60%), below which all substrates are listed as 'no confident result' although the best prediction is still provided to the user.

AdenylPred availability The web application built using RShiny is available at z.umn.edu/adenylpred. The command-line version of the tool is available at https://github.com/serina-robinson/adenylpred/.

Phylogenetic analysis and ancestral reconstruction Training set sequences were aligned were aligned using HMMAlign (*49*) and terminal ends of the alignment were trimmed. The phylogeny of the entire training set was estimated using RAxML (*51*) using the Jones-Taylor-Thornton matrix-based model of amino acid substitution and a discrete gamma model with 20 rate categories. For ancestral sequence reconstruction, training set sequences were redundancy filtered to 40% amino acid identity with a word size of 2 using CD-HIT (*47*). FastML was used to reconstruct the most likely ancestral sequences for internal nodes of the tree (*19*).

AdenylPred was then used to predict the functional class and substrate of the root ancestral sequence.

HPLC analysis of NltC activity High-performance liquid chromatography (HPLC) analysis of ATP, ADP, and AMP was conducted using an Agilent 1100 series instrument with a C_{18} eclipse plus (Agilent) column mounted with a C_{18} guard column. Reactions were carried out in glass HPLC vials with a total volume of 500 µL in assay buffer (50 mM Tris base adjusted to pH 8.0 with HCl). Reactions were initiated with the addition of 0.5 µM enzyme (15 µg) to 100 µM of ATP, 100 µM of substrate, and 2% EtOH originating from the substrate stocks. Separation of ATP, ADP, and AMP was observed after 9 min under isocratic conditions with 95% 100 mM H_2KPO_4 (pH 6.0 with KOH) and 5% methanol while monitoring at 259 nm.

Cloning, Expression, and Purification of Nocardiolactone Biosynthetic Enzymes NltA (WP_042260942.1), NltB (WP_042260944.1), NltC (WP_042260945.1) and NltD (WP_042260949.1) from *Nocardia brasiliensis* and NltA from *Nocardia yamanshiensis* (WP_067710538.1), were codon-optimized for *E. coli* and synthesized by Integrated DNA Technologies (IDT, USA). NltC was cloned into a pET30b+ vector with NdeI and XhoI restriction sites with a C-terminal 6-histidine tag. NltD was cloned into a modified pMAL-c5x vector with a tobacco etch virus protease cut site added at NdeI and XhoI restriction sites and a N-terminal 6-histidine tag and expressed as a fusion with maltose binding protein. NltA from *N. yamanashiensis* was cloned into a pET28b+ at NdeI and XhoI restriction sites. NltA and NltB from *N. brasiliensis* were cloned both individually as in the case of *N. yamanashiensis* and together with a ribosome binding site inserted between into a single pET28b+ vector with a N-terminal 6-histidine tag. Constructs were cloned by Gibson assembly and verified by Sanger sequencing. All vectors were transformed into BL21 (DE3) cells (NEB). Starter cultures (5 mL) were grown in Terrific Broth overnight at 37° C with kanamycin selection. 1-Liter cultures with 75 µg/ml kanamycin were grown to an optical density of 0.5 at 37° C, induced by addition of 1 mL isopropyl β-D-1-thiogalactopyranoside (IPTG, 1 M stock) and further incubated for 19 h at 15°C. Induced cells were harvested at 4000 x g with a Beckman centrifuge and frozen at −80 °C. Cell pellets were resuspended in 10 mL of buffer containing 500 mM NaCl, 20 mM Tris base, and 10% glycerol at pH 7.4. Elution buffer for the nickel column was the same but with the addition of 400 mM imidazole. NltD purification buffer had the addition of 0.025% Tween 20. Cell pellets were thawed on ice, lysed with 2–3 cycles in a French pressure cell (1500 pounds per square inch) and centrifuged for 60 min at 17,000 x g. Supernatants were filtered through a 0.45 µM low protein binding filter (Corning, USA), loaded into a GE Life Sciences ÄKTA fast liquid protein chromatography system and injected onto a GE Life Sciences HisTrap HP 5 ml column. After washes to remove nonspecifically bound proteins, his-tagged proteins were eluted with a stepwise gradient of 5, 10, 15, and 80% elution buffer over 2.5 column volumes at 1 ml/min and collected in 2 ml fractions. Protein concentration was determined by the method of Brasford (*52*) using the Bio-Rad (USA) Protein Assay Dye Reagent Concentrate and a standard curve prepared from a 2 mg/mL bovine albumin standard (Thermo Scientific). The desired protein fractions were pooled, analyzed by SDS-PAGE, flash frozen in liquid N_2 and stored at -80 °C.

GC-MS Separation and identification of metabolites was accomplished by gas chromatography/mass spectrometry (GC-MS Agilent 7890a & 5975c) equipped with an Agilent J&W DB1-ms column (30 m, 0.25 mm diameter,
0.25 µm film). The formation of the unstable β-keto acid catalyzed by OleA and NltAB could be observed as its ketone breakdown product by GC-MS as published previously *(31)*. Olefin (from either β-lactone breakdown or standards) was detected without derivatization, but the β-hydroxy acid required methylation of the carboxylic acid group by diazomethane. Preparation of ethereal alcoholic solutions of diazomethane from N-methyl-N-nitroso-p-toluenesulfonamide was carried out using a commercial kit from Aldrich (Technical information Bulletin No. Al-113). All samples were extracted with tert-methyl butyl ether and mixed with 50 µL of diazomethane solution. One microliter of each sample was injected into the

injection port (230° C). The 25 min program was as follows: hold 80° C for 2 min; ramp linearly to 320° C for 20 min; hold 320° C for 3 min.

Verification of NltC β-lactone synthetase activity by ^{1}H-NMR Reaction mixtures contained 1.0 mg NltC, 20 mg ATP, and 30 mg $MgCl_2 \cdot 6H_2O$ in 100 mL of 200mM NaCl and 20 mM $NaPO_4$ buffer at pH 7.4. 2-octyl-3-hydroxydodecanoic acids were dissolved in EtOH to 1.0 mg/mL, and 1-bromo-napthalene at 0.5 mg/mL was included as an internal standard. Reactions were initiated with 1.5 mL of EtOH-substrate solution and allowed to run for 24 hours before three successive extractions were performed with 10 mL, 5 mL, and 5 mL of dichloromethane. Samples were allowed to evaporate at room temperature before dissolving in $CDCl_3$ for ^{1}H-NMR (400 MHz). Figure S4A shows the ^{1}H-NMR spectra of NltC β-lactone synthetase reactions compared to a no enzyme control.

NltD activity assay Activity of NltD/OleD by NADPH-dependent consumption of 2-alkyl-3-ketoalkanoic acid was monitored using the method described by Bonnett et al. (*30*). The reaction was measured in reverse since the keto acid substrate for NltD/OleD homologs was previously shown to be unstable and spontaneously decarboxylates to a ketone *(30)*. Briefly, progress was tracked by the change in absorbance at 340 nm by the formation or consumption of NADPH (ε_{340} = 6,220 M^{-1} cm^{-1}) in UV-transparent 96 well plates (Greiner, Sigma-Aldrich) and monitored using a SpectraMax Plus microplate reader (Molecular Devices).

General synthetic procedures Synthesis and purification of racemic 2-octyl-3-hydroxydodecanoic acid was performed as described previously (*8, 53*) via *α*-carbon deprotonation of decanoic acid by lithium diisopropylamide (LDA) followed by the addition of decanal to form 2-octyl-3-hydroxydodecanoate. An identical synthetic method was used to synthesize a racemic diastereomeric mix of 2-hexyl-3-hydroxyoctanoic acid from hexanal and octanoic acid as described by Robinson et al. (*27*).

Declaration of Interests
M.H.M. is on the scientific advisory board of Hexagon Bio.

Author Contributions
Conceptualization, S.L.R., M.H.M, and L.P.W.; Methodology, S.L.R., B.R.T. M.H.M, and L.P.W.; Software, S.L.R. and B.R.T.; Validation, S.L.R., B.R.T., S.J.P., and M.D.S.; Formal Analysis, S.L.R. and B.R.T.; Investigation, S.L.R., S.J.P. and M.D.S.; Data Curation, S.L.R. and B.R.T.; Writing – Original Draft, S.L.R.; Writing – Review & Editing, S.L.R., B.R.T., S.J.P, T.S., M.H.M., and L.P.W.; Supervision – M.H.M. and L.P.W.

Acknowledgements
We acknowledge Satria Kautsar for assistance in extracting candidate biosynthetic gene clusters. Aalt-Jan van Dijk is recognized for his insightful discussions on machine learning. Kelly Aukema is acknowledged for manuscript edits and discussion. We are grateful to Jorge Navarro Muñoz for providing the output from fungiSMASH analysis. S.L.R. is supported by the National Science Foundation (NSF) Graduate Research Fellowship (Grant no. 00039202) and a Graduate Research Opportunities Worldwide (GROW) fellowship to the Netherlands.

References
1. Lipmann, F. Enzymatic synthesis of acetyl phosphate. *Journal of Biological Chemistry*. 1944;155:55-70

2. Gulick, A.M. Conformational dynamics in the acyl-Coa synthetases, adenylation domains of non-ribosomal peptide synthetases, and firefly luciferase. *ACS Chemical Biology.* 2009;4(10):811-827.

3. Wang N, Rudolf JD, Dong LB, et al. Natural separation of the acyl-CoA ligase reaction results in a non-adenylating enzyme. *Nature Chemical Biology.* 2018;14(7):730-+.

4. Bera AK, Atanasova V, Gamage S, Robinson H, Parsons JF. Structure of the D-alanylgriseoluteic acid biosynthetic protein EhpF, an atypical member of the ANL superfamily of adenylating enzymes. *Acta Crystallographica Section D-Biological Crystallography.* 2010;66:664-672.

5. Arora P, Goyal A, Natarajan VT, et al. Mechanistic and functional insights into fatty acid activation in *Mycobacterium tuberculosis*. *Nature Chemical Biology.* 2009;5(3):166-173.

6. Cimermancic P, Medema MH, Claesen J, et al. Insights into Secondary Metabolism from a Global Analysis of Prokaryotic Biosynthetic Gene Clusters. *Cell.* 2014;158(2):412-421.

7. Schoner TA, Fuchs SW, Schonau C, Bode HB. Initiation of the flexirubin biosynthesis in *Chitinophaga pinensis*. *Microbial Biotechnology.* 2014;7(3):232-241.

8. Christenson JK, Richman JE, Jensen MR, Neufeld JY, Wilmot CM, Wackett LP. β-Lactone synthetase found in the olefin biosynthesis pathway. *Biochemistry.* 2017;56(2):348-351.

9. Waldman AJ, Balskus EP. Discovery of a diazo-forming enzyme in cremeomycin biosynthesis. *Journal of Organic Chemistry.* 2018;83(14):7539-7546.

10. Khurana P, Gokhale RS, Mohanty D. Genome scale prediction of substrate specificity for acyl adenylate superfamily of enzymes based on active site residue profiles. *BMC Bioinformatics.* 2010;11:17.

11. Röttig M, Medema MH, Blin K, Weber T, Rausch C, Kolbacher O. NRPSpredictor2-a web server for predicting NRPS adenylation domain specificity. *Nucleic Acids Research.* 2011;39:W362-W367.

12. Chevrette MG, Aicheler F, Kohlbacher O, Currie CR, Medema MH. SANDPUMA: ensemble predictions of nonribosomal peptide chemistry reveal biosynthetic diversity across Actinobacteria. *Bioinformatics.* 2017;33(20):3202-3210.

13. Pan GH, Xu ZR, Guo ZK, et al. Discovery of the leinamycin family of natural products by mining actinobacterial genomes. *Proceedings of the National Academy of Sciences of the United States of America.* 2017;114(52):E11131-E11140.

14. Zhao H, Liu YP, Zhang LQ. In silico and genetic analyses of cyclic lipopeptide synthetic gene clusters in *Pseudomonas* sp. 11K1. *Frontiers in Microbiology.* 2019;10:11.

15. Kautsar, SA, Blin, K, Shaw, S, Navarro-Muñoz, JC, Terlouw, BR, van der Hooft, JJ, van Santen, J, Tracanna, V, Suarez Duran, HG, Andreu, VP, Selem-Mojica, N, Alanjary, M, Robinson, SL, Lund, G, Epstein, SC, Sisto, AC, Charkoudian, LK, Collemare, J, Linington, R, Weber, T, Medema, MH. MIBiG 2.0: a repository for biosynthetic gene clusters of known function. *Nucleic Acids Research.* 2019; doi:10.1093/nar/gkz882.

16. Bateman A, Martin MJ, Orchard S, et al. UniProt: a worldwide hub of protein knowledge. *Nucleic Acids Research.* 2019;47(D1):D506-D515.

17. Fujino T, Kang MJ, Suzuki H, Iijima H, Yamamoto T. Molecular characterization and expression of rat acyl-CoA synthetase 3. *Journal of Biological Chemistry.* 1996;271(28):16748-16752.

18. Akiva E, Copp JN, Tokuriki N, Babbitt PC. Evolutionary and molecular foundations of multiple contemporary functions of the nitroreductase superfamily. *Proceedings of the National Academy of Sciences of the United States of America.* 2017;114(45):E9549-E9558.

19. Ashkenazy H, Penn O, Doron-Faigenboim A, Cohen O, Cannarozzi G, Zomer O, Pupko T. FastML: a web server for probabilistic reconstruction of ancestral sequences. *Nucleic Acids Research*. 2012;40(W1):W580-4.

20. Blin K, Shaw S, Steinke K, Villebro R, Ziemert N, Lee SY, Medema MH, Weber T. antiSMASH 5.0: updates to the secondary metabolite genome mining pipeline. *Nucleic Acids Research.* 2019. 10.1093/nar/gkz310

21. Blin K, Wolf T, Chevrette MG, et al. antiSMASH 4.0-improvements in chemistry prediction and gene cluster boundary identification. *Nucleic Acids Research.* 2017;45(W1):W36-W41.

22. Kautsar SA, Duran HGS, Blin K, Osbourn A, Medema MH. plantiSMASH: automated identification, annotation and expression analysis of plant biosynthetic gene clusters. *Nucleic Acids Research.* 2017;45(W1):W55-W63.

23. Galica T, Hrouzek P, Mares J. Genome mining reveals high incidence of putative lipopeptide biosynthesis NRPS/PKS clusters containing fatty acyl-AMP ligase genes in biofilm-forming cyanobacteria. *Journal of Phycology.* 2017;53(5):985-998.

24. Bai T, Zhang D, Lin S, Long Q, Wang Y, Ou H, Kang Q, Deng Z, Liu W, Tao M. Operon for biosynthesis of lipstatin, the β-lactone inhibitor of human pancreatic lipase. *Applied and Environmental Microbiology.* 2014;80(24):7473-83.

25. Wyatt MA, *et al.*, Biosynthesis of ebelactone A: isotopic tracer, advanced precursor and genetic studies reveal a thioesterase-independent cyclization to give a polyketide beta-lactone. *Journal of Antibiotics.* 2013;66, 421-430.

26. Mikami Y, Yazawa Y, Tanaka Y, Ritzau M, Grafe U. Isolation and structure of nocardiolactone, a new dialkyl-substituted beta-lactone from pathogenic *Nocardia* strains. *Natural Product Letters.* 1999;13(4):277-284.

27. Robinson SL, Christenson JK, Richman JE, et al. Mechanism of a standalone β-lactone synthetase: New continuous assay for a widespread ANL superfamily enzyme. *ChemBioChem.* 2019;20:1701-1711.

28. Zhang D, Zhang F, Liu W. A KAS-III heterodimer in lipstatin biosynthesis nondecarboxylatively condenses C_8 and C_{14} fatty acyl-CoA substrates by a variable mechanism during the establishment of a C_{22} aliphatic skeleton. *Journal of the American Chemical Society.* 2019;141(9):3993-4001.

29. Goblirsch BR, Jensen MR, Mohamed FA, Wackett LP, Wilmot CM. Substrate trapping in crystals of the thiolase OleA identifies three channels that enable long chain olefin biosynthesis. *Journal of Biological Chemistry.* 2016;291(52):26698-26706.

30. Bonnett SA, Papireddy K, Higgins S, del Cardayre S, Reynolds KA. Functional characterization of an NADPH dependent 2-alkyl-3-ketoalkanoic acid reductase involved in olefin biosynthesis in *Stenotrophomonas maltophilia*. *Biochemistry.* 2011;50(44):9633-40.

31. Frias JA, Richman JE, Erickson JS, Wackett LP. Purification and Characterization of OleA from *Xanthomonas campestris* and demonstration of a non-decarboxylative Claisen condensation reaction. *Journal of Biological Chemistry.* 2011;286(13):10930-10938.

32. Wattam AR, Abraham D, Dalay O, et al. PATRIC, the bacterial bioinformatics database and analysis resource. *Nucleic Acids Research.* 2014;42(D1):D581-D591

33. Baier F, Tokuriki N. Connectivity between catalytic landscapes of the metallo-β-lactamase superfamily.

Journal of Molecular Biology. 2014;426(13):2442-56.

34. Hicks MA, Barber AE, Giddings LA, Caldwell J, O'Connor SE, Babbitt PC. The evolution of function in strictosidine synthase-like proteins. *Proteins: Structure, Function, and Bioinformatics*. 2011 Nov;79(11):3082-98.

35. Linne U, Schafer A, Stubbs MT, Marahiel MA. Aminoacyl-coenzyme A synthesis catalyzed by adenylation domains. *FEBS Letters.* 2007;581(5):905-910.

36. Oba Y, Ojika M, Inouye S. Firefly luciferase is a bifunctional enzyme: ATP-dependent monooxygenase and a long chain fatty acyl-CoA synthetase. *FEBS Letters.* 2003;540(1-3):251-254.

37. Oba Y, Iida K, Inouye S. Functional conversion of fatty acyl-CoA synthetase to firefly luciferase by site-directed mutagenesis: A key substitution responsible for luminescence activity. *FEBS Letters.* 2009;583(12):2004-2008.

38. Robinson SL, Christenson JK, Wackett LP. Biosynthesis and chemical diversity of β-lactone natural products. *Natural Product Reports*. 2019;36(3):458-75.

39. Wang Y, Tennyson RL, Romo D. β-Lactones: intermediates for natural product total synthesis and new transformations. *Heterocycles*. 2004;64(1):605-58.

40. Allemann MN, Shulse CN, Allen EE. Linkage of marine bacteria polyunsaturated fatty acid and long-chain hydrocarbon biosynthesis. *Frontiers in Microbiology.* 2019;10:10.

41. Komaki H, Ichikawa N, Hosoyama A, et al. Genome based analysis of type-I polyketide synthase and nonribosomal peptide synthetase gene clusters in seven strains of five representative *Nocardia* species. *BMC Genomics.* 2014;15:11.

42. Pidot SJ, Herisse M, Sharkey L, et al. Biosynthesis and ether-bridge formation in nargenicin macrolides. *Angewandte Chemie-International Edition.* 2019;58(12):3996-4001.

43. Kuo J, Lynch SR, Liu CW, Xiao XR, Khosla C. Partial in vitro reconstitution of an orphan polyketide synthase associated with clinical cases of nocardiosis. *ACS Chemical Biology.* 2016;11(9):2636-2641.

44. Trevino-Villarreal JH, Vera-Cabrera L, Valero-Guillén PL, Salinas-Carmona MC. *Nocardia brasiliensis* cell wall lipids modulate macrophage and dendritic responses that favor development of experimental actinomycetoma in BALB/c mice. *Infection and Immunity*. 2012;80(10):3587-601.

45. Beaman BL. Differential binding of *Nocardia asteroides* in the murine lung and brain suggests multiple ligands on the nocardial surface. *Infection and immunity*. 1996;64(11):4859-62.

46. Blin K, Andreu VP, de los Santos ELC, et al. The antiSMASH database version 2: a comprehensive resource on secondary metabolite biosynthetic gene clusters. *Nucleic Acids Research.* 2019;47(D1):D625-D630.

47. Fu LM, Niu BF, Zhu ZW, Wu ST, Li WZ. CD-HIT: accelerated for clustering the next-generation sequencing data. *Bioinformatics.* 2012;28(23):3150-3152.

48. Csardi G, Nepusz T. The igraph software package for complex network research. *InterJournal.* 2006;1695(5):1-9.

49. Eddy SR. Accelerated profile HMM searches. *PLOS Computational Biology.* 2011;7(10):16.

50. Malley JD, Kruppa J, Dasgupta A, Malley KG, Ziegler A. Probability machines. *Methods of Information in Medicine.* 2012;51(01):74-81.

51. Stamatakis A. RAxML version 8: a tool for phylogenetic analysis and post-analysis of large phylogenies. *Bioinformatics*. 2014;30(9):1312-3.

52. Brasford MM. A rapid and sensitive method for quantitation of microgram quantities of protein utilizing the principle of protein-dye binding. *Analytical Biochemistry*. 1976;72:248-54.

53. Mulzer J, Brüntrup G, Hartz G, Kühl U, Blaschek U, Böhrer G. Additionen von Carbonsäure-Dianionen an α, β-ungesättigte Carbonylverbindungen-Steuerung der 1, 2-/1, 4-Regioselektivität durch sterische Substituenteneffekte. *Chemische Berichte.* 1981;114(11):3701-3724.

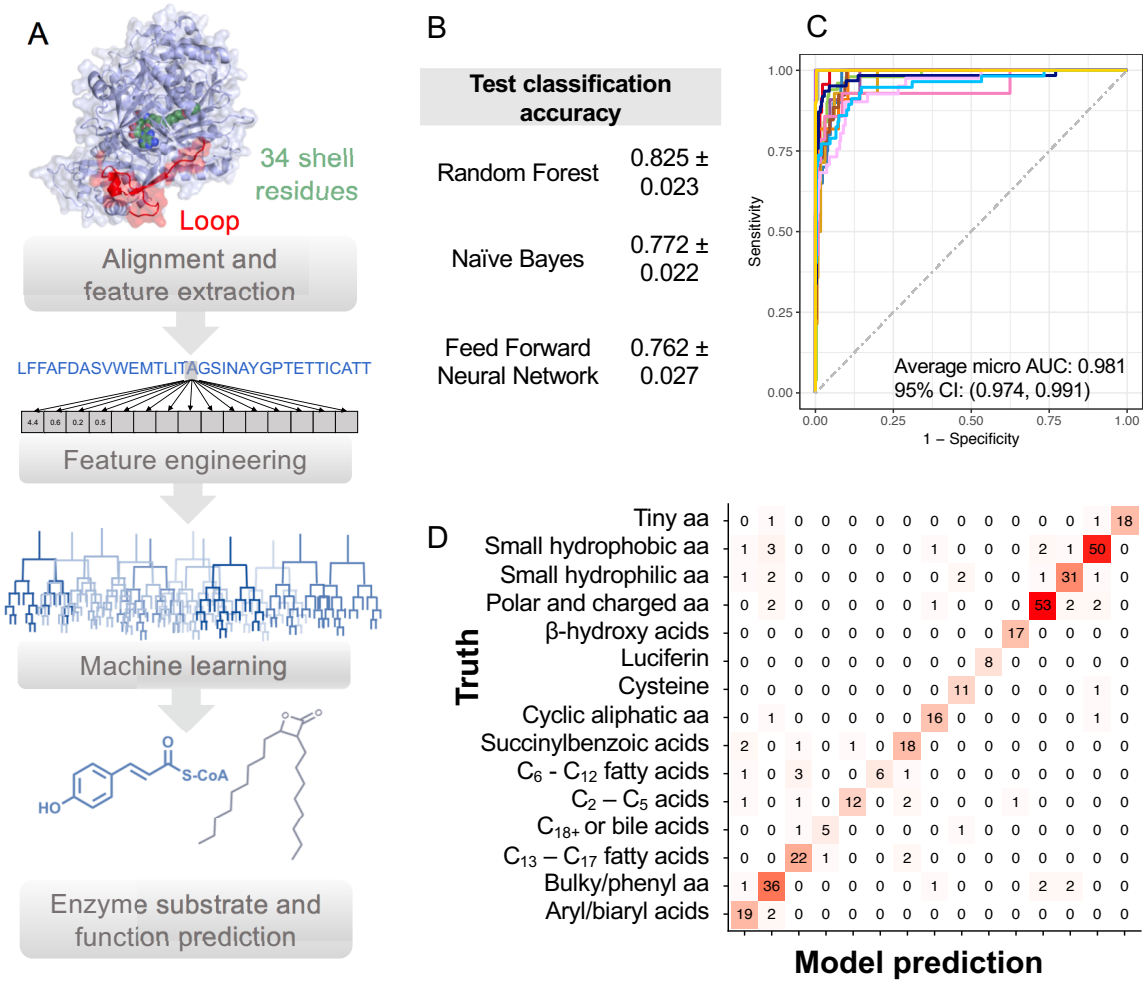

Figure 1. A) Workflow to predict substrate and function of adenylate-forming enzymes from protein sequence inputs. 34 active site residues (green) and FAAL-specific loop (red) residues are extracted and encoded as a vector of physiochemical properties specific to each amino acid. Separate classifiers are trained to predict substrate specificity and enzyme function. B) Hold-out test set accuracy for three different classification methods evaluated in this study C) Area under the receiver operating characteristics curve for substrate specificity predictions. Colors correspond to different substrates. D) Confusion matrix of predicted vs. truth for ANL substrate specificity on hold-out test set. aa = amino acids. Functional predictions are presented in Figure S3.

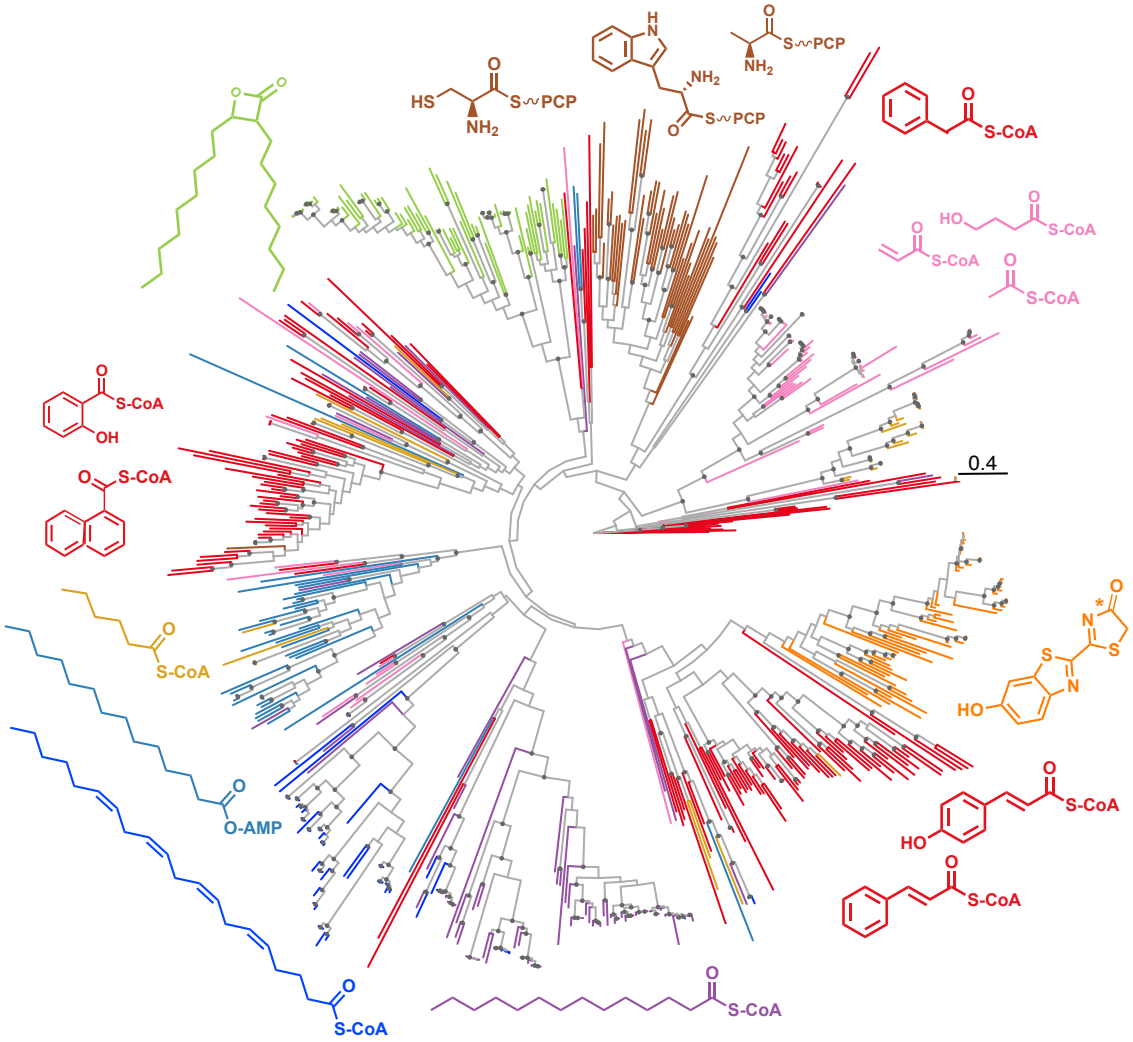

Figure 2. Maximum-likelihood tree of characterized protein sequences in the ANL superfamily computed using the Jones-Taylor-Thornton matrix-based model of amino acid substitution and colored by functional enzyme class. Some enzyme classes such as BLS, NRPS, and LUC form monophyletic clades while other sequences i.e. the ARYL class are dispersed throughout the tree, suggesting evolutionary divergence. Red = ARYL, Green = BLS, Dark blue = VLACS, Orange = LUC, Light blue = FAAL, Brown = NRPS, Purple = LACS, Pink = SACS, Gold = MACS. Gray node circles represent bootstrap support >75 at branch points. Bar, 0.4 aa substitutions per site.

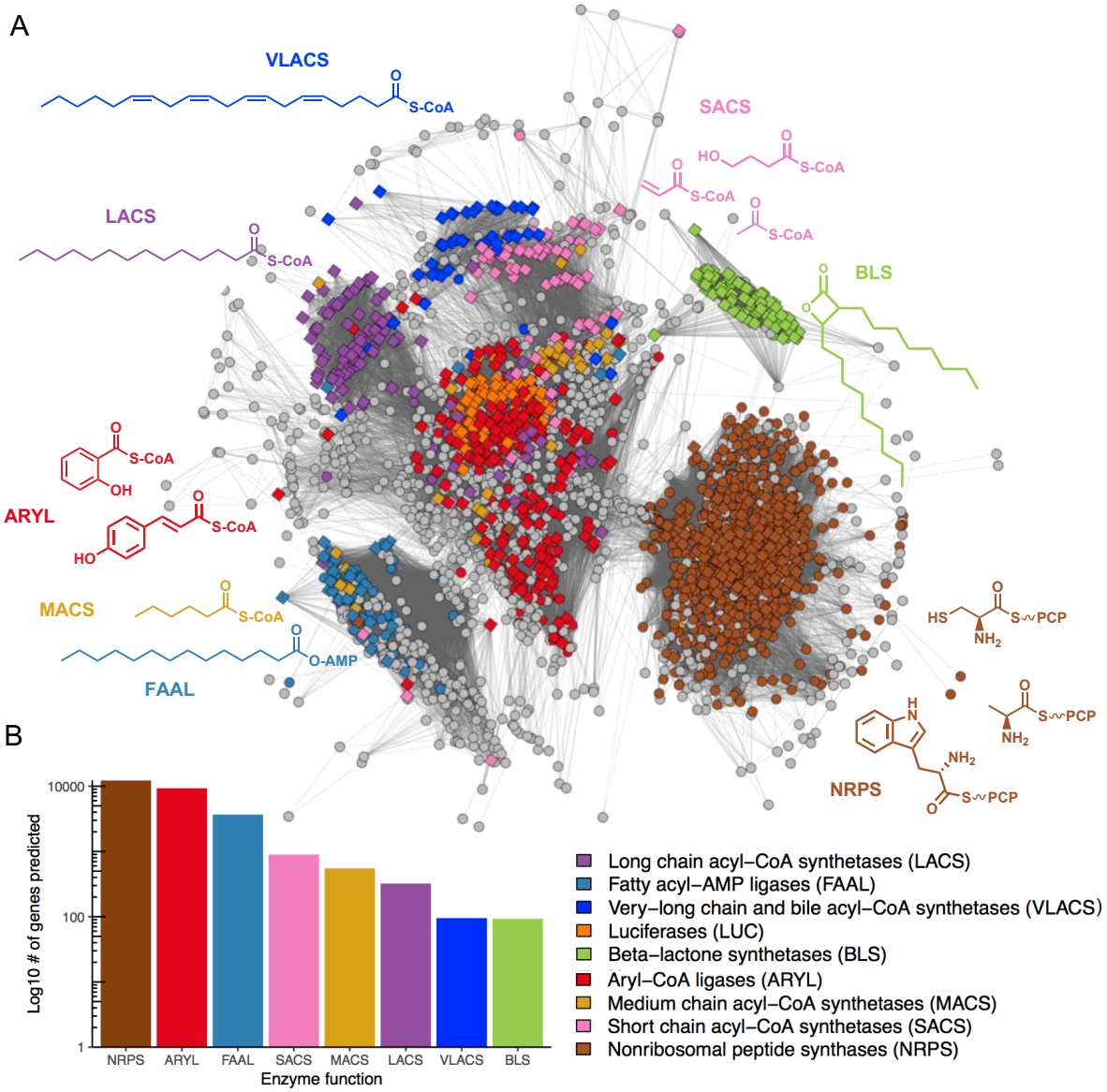

Figure 3. A) Sequence similarity network of all AMP-binding pHMM hits from 50,064 predicted biosynthetic gene clusters in bacterial, fungal, and plant genomes. Diamonds correspond to training set sequences and circles represent AMP-binding hits extracted from biosynthetic gene clusters. The network was trimmed to a BLAST e-value threshold of 1 x 10^{-36}. Circles with a probability > 0.6. are colored by their prediction, while sequences colored gray have 'no confident prediction.' B) Bar plot of relative distribution of functional classes of ANL enzymes within biosynthetic gene clusters (AdenylPred prediction probability > 0.6).

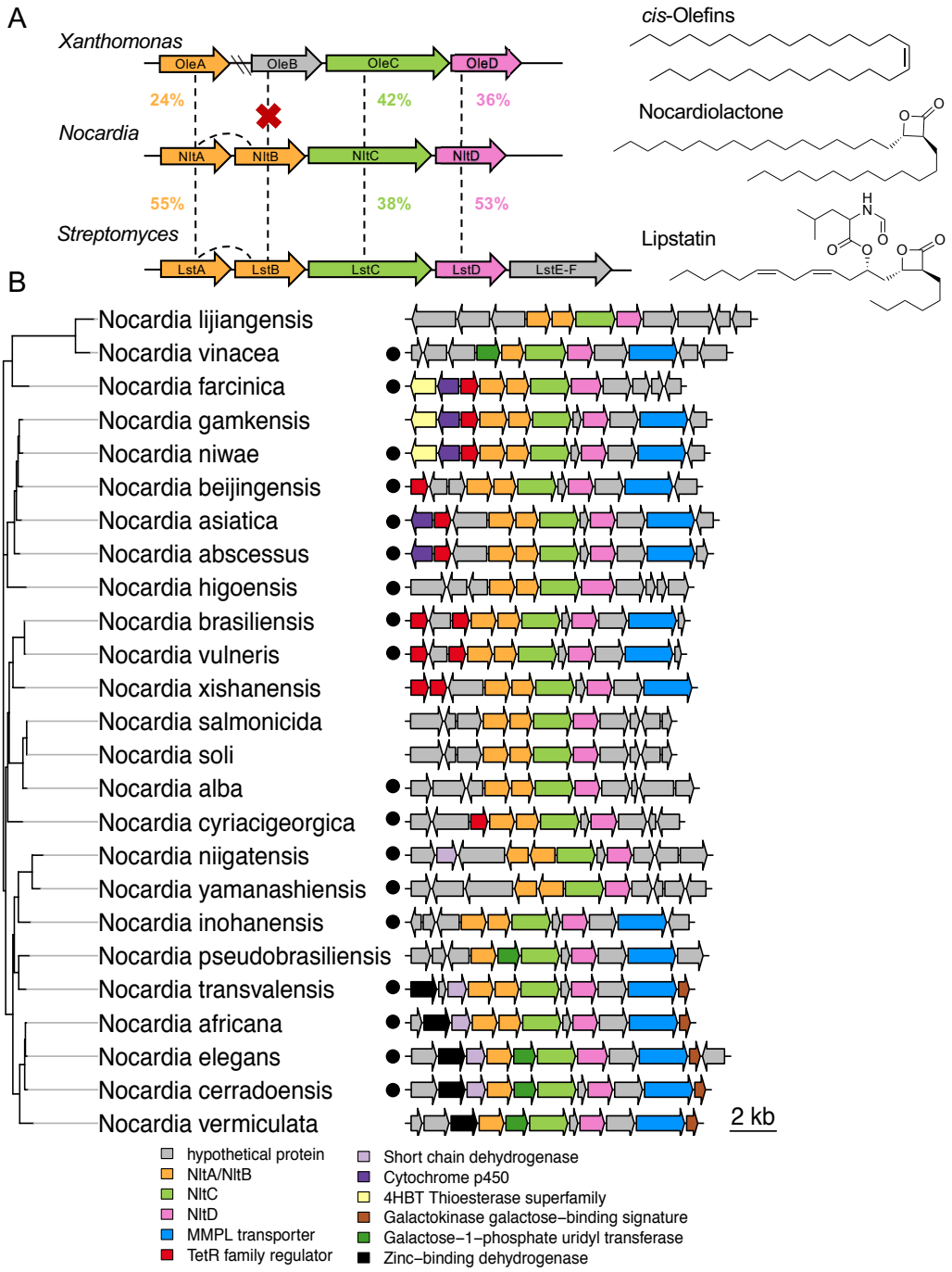

Figure 4. A) Synteny between bacterial *cis*-olefin and lipstatin gene clusters with the nocardiolactone biosynthetic gene cluster proposed here. Percentages correspond to amino acid (aa) identity. B) Representative examples of the proposed nocardiolactone biosynthetic cluster across different species of *Nocardia.* Maximum-likelihood phylogenetic tree is based on NltC amino acid sequence distance estimated using the Jones Taylor-Thornton model of amino acid substitution. Sequences corresponding to *Nocardia* isolated from human patients are designated by black circles.

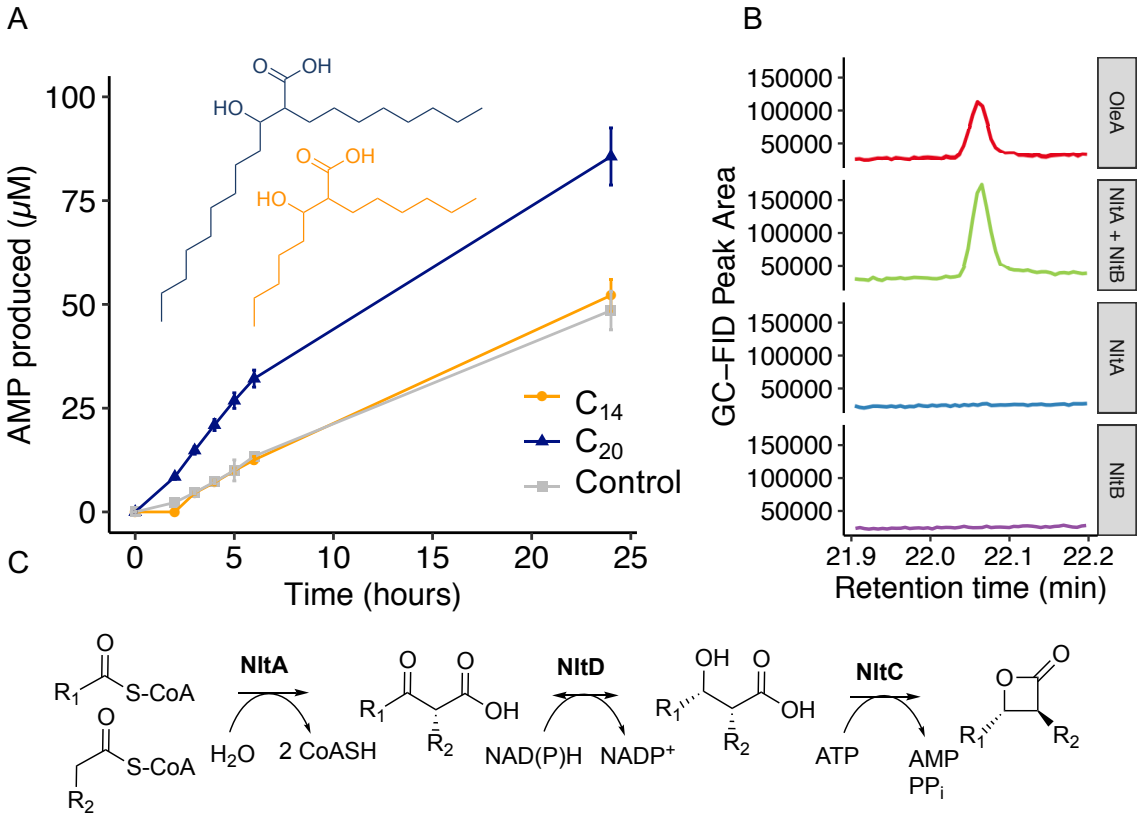

Figure 5. A) Time-course analysis of NltC activity with di-alkyl β-hydroxy acids with carbon backbones of length C_{20} (blue) and C_{14} (orange) compared to a no substrate control (gray). NltC prefers longer chain (C_{20}) and shows no discernable activity with C_{14} above the level of the no substrate control. B) Co-expressed NltA and NltB condense 2 myristoyl-CoAs to form 2-myristoyl-3-ketomyristic acid. The resulting ketone (14-heptacosanone) from the breakdown of 2-myristoyl-3-ketomyristic acid was observed by GC-MS. The enzymatic product of NltA and NltB was identical to a 14-heptacosanone control produced by wild-type *X. campestris* OleA but was not observed to be catalyzed by NltA or NltB enzymes purified individually. C) Proposed biosynthetic pathway for nocardiolactone. $R_1 = C_{18}H_{37}$, $R_2 = C_{13}H_{27}$.